Electronic Supporting Information

Bimetallic CoSn nanoparticles anchored on N-doped carbon as antibacterial oxygen reduction catalysts for microbial fuel cells

Liang Li[a,b], Zequan Liu[c], Demin Jiang[a], Min Song[*c], Yuqiao Wang[*a,b]

[a.] Research Center for Nano Photoelectrochemistry and Devices, School of Chemistry and Chemical Engineering, Southeast University, Nanjing 211189, China

[b.] Yangtze River Delta Carbon Neutrality Strategy Development Institute, Southeast University, Nanjing 210096, China

[c.] School of Energy and Environment, Southeast University, Nanjing 210096, China

[*]Corresponding author (Email: minsong@seu.edu.cn; yqwang@seu.edu.cn).

Materials characterization

The X-ray diffraction spectrum (XRD, Ultima IV) was applied to characterize the crystallinity of the synthesized samples in the 2-theta range of 10-80°. The X-ray photoelectron spectroscopy (XPS, K-Aepna, Thermo Fisher Scientific Inc., USA) was used to obtain the information of the element composition of different catalysts. Scanning electron microscope (SEM, FEI inspect F50), transmission electron microscope (TEM, JEM-2100F, JEOL, Japan) and high-resolution TEM (HRTEM, JEM-2100F, JEOL, Japan) were used to observe the morphology of different catalysts.

DFT calculation

To predict ORR performance, DFT theory calculation was carried out by four elementary steps as follows[20]:

$$\text{OOH formation: } O_2^* + H_2O + e^- \rightarrow OOH^* + OH^- \qquad (1)$$

$$\text{OOH dissociation: } OOH^* + e^- \rightarrow O^* + OH^- \qquad (2)$$

O hydration: $O^* + H_2O + e^- \rightarrow OH^* + OH^-$ (3)

OH desorption: $OH^* + e^- \rightarrow OH^- + *$ (4)

Note that * denoted the reaction site of materials.

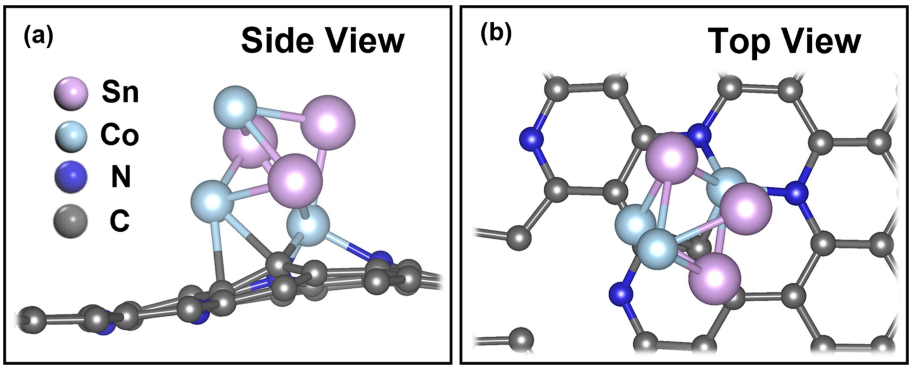

Fig. S1 Side view (a) and top view (b) of optimized structures of CoSn@NC.

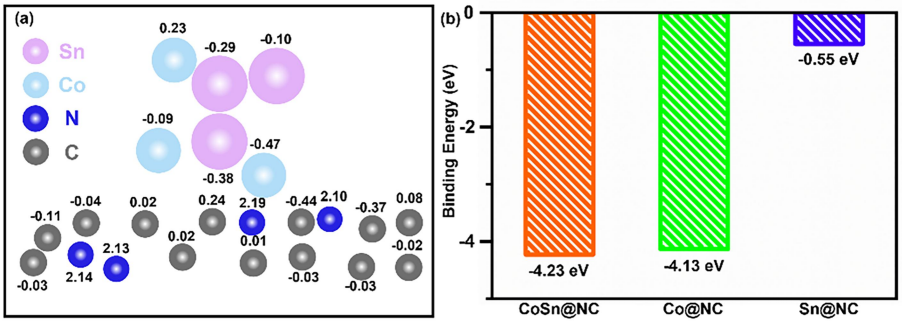

Fig. S2 (a) Calculated charge of atoms of CoSn@NC, (b) The binding energy of nanoparticles and NC for different catalysts.

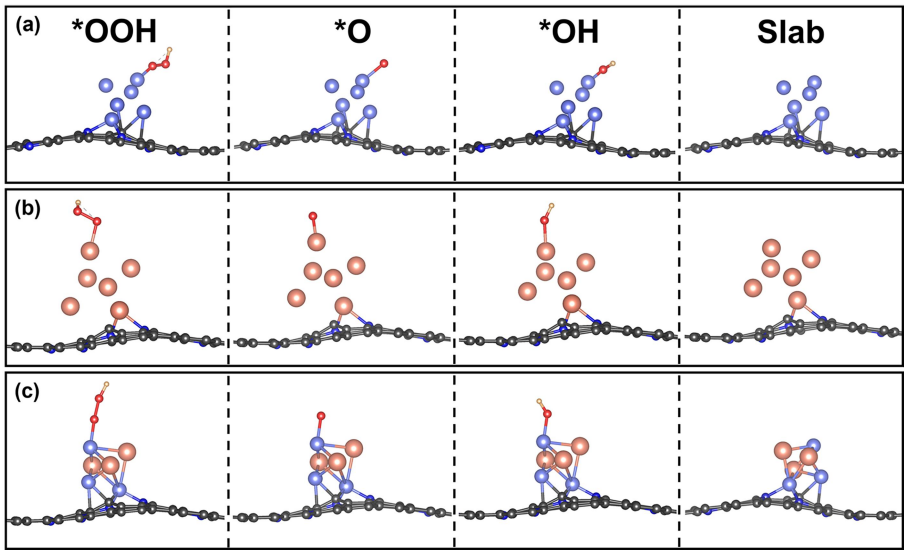

Fig. S3 Structure models for the adsorbed intermediates *OOH, *O, *OH and slab at the interface of (a) Co@NC, (b) Sn@NC, (c) CoSn@NC in alkaline media during the ORR. (Orange atom: Sn, light blue atom: Co, blue atom: N, gray atom: C, red atom: O, yellow atom: H)

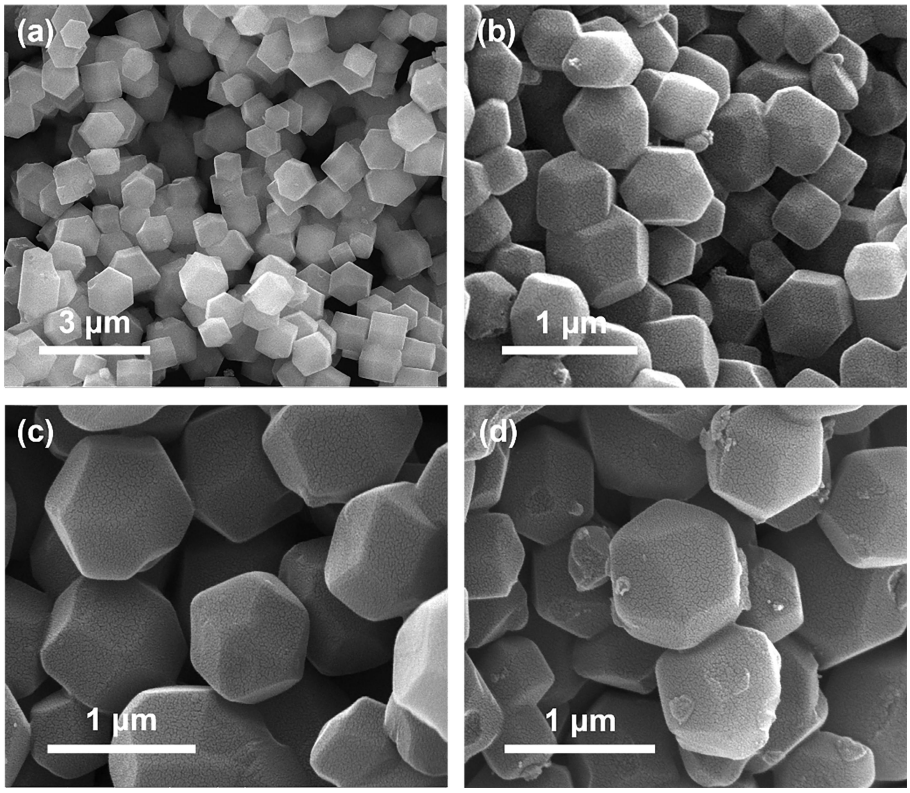

Fig. S4 SEM images of (a) ZIF precursor, (b) NC, (c) Co@NC, (d) Sn@NC.

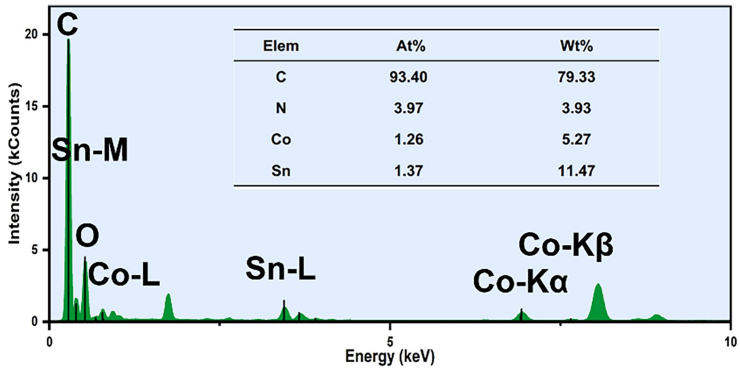

Elem	At%	Wt%
C	93.40	79.33
N	3.97	3.93
Co	1.26	5.27
Sn	1.37	11.47

Fig. S5 EDS patterns of CoSn@NC.

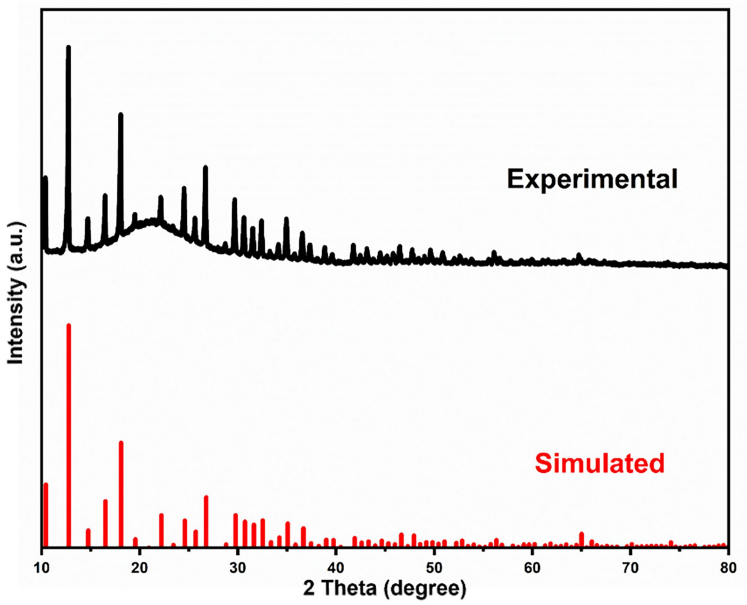

Fig. S6 XRD patterns of ZIF precursor.

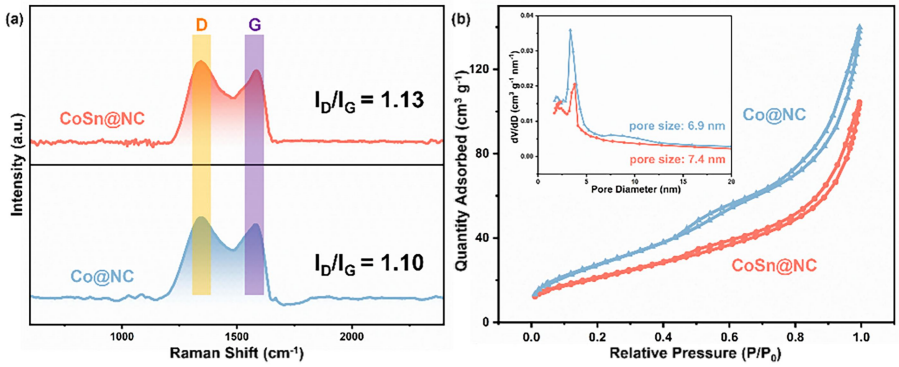

Fig. S7 (a) Raman spectra of Co@NC and CoSn@NC. (b) N_2 adsorption-desorption isotherms and pore size distrebutions.

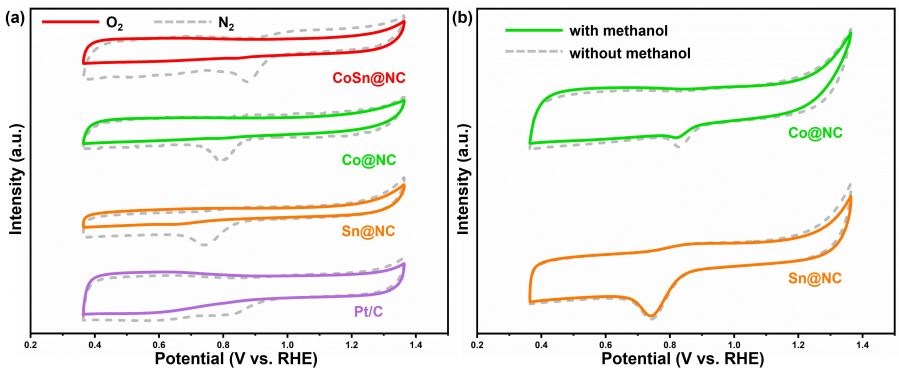

Fig. S8 (a) CV curves of different catalysts in N_2-saturated 0.1 M KOH. (b) The resistance to poisoning of Co@NC and Sn@NC.

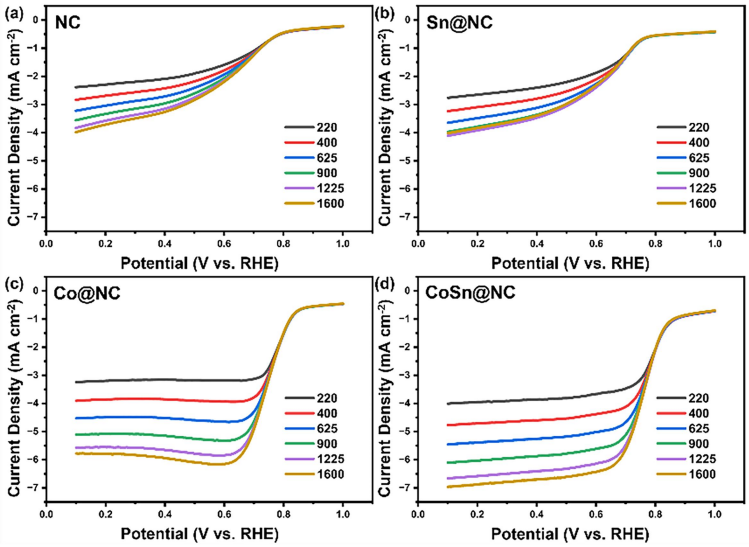

Fig. S9 LSV curves of catalysts in 0.1 M KOH with different electrode rotation speeds.

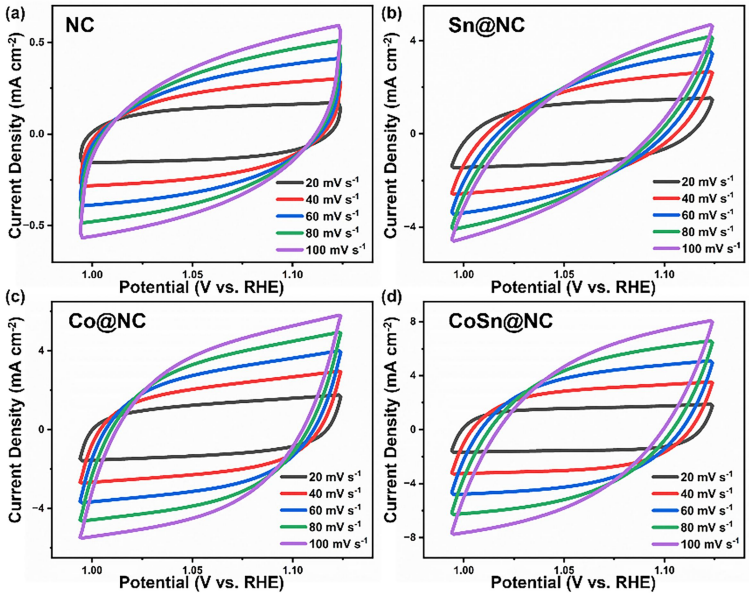

Fig. S10 CV curves of (a) NC, (b) Sn@NC, (c) Co@NC and (d) CoSn@NC in the non-faradic capacitance current range from 20 to 100 mV s^{-1}.

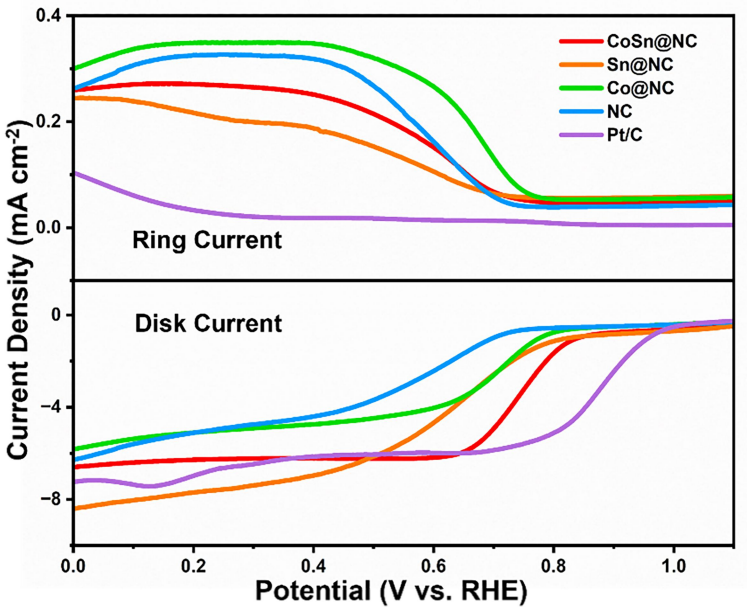

Fig. S11 Ring currents and disk currents collected in the RRDE systems.

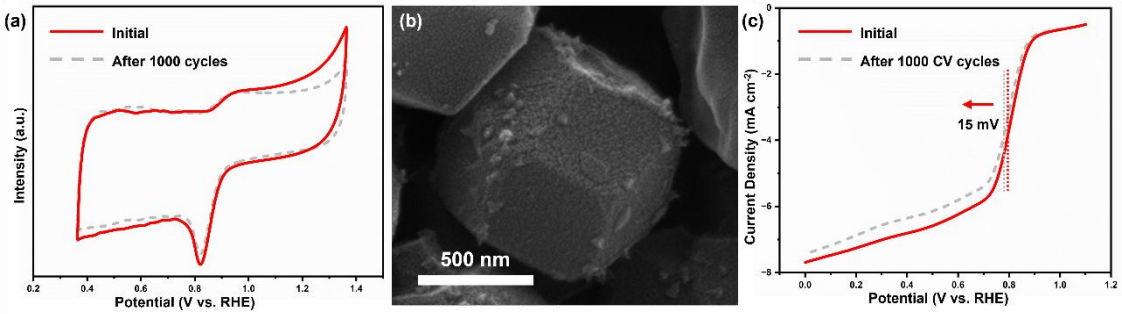

Fig. S12 CV curves (a), SEM image (b) and LSV curves (c) of CoSn@NC after 1000 cycles.

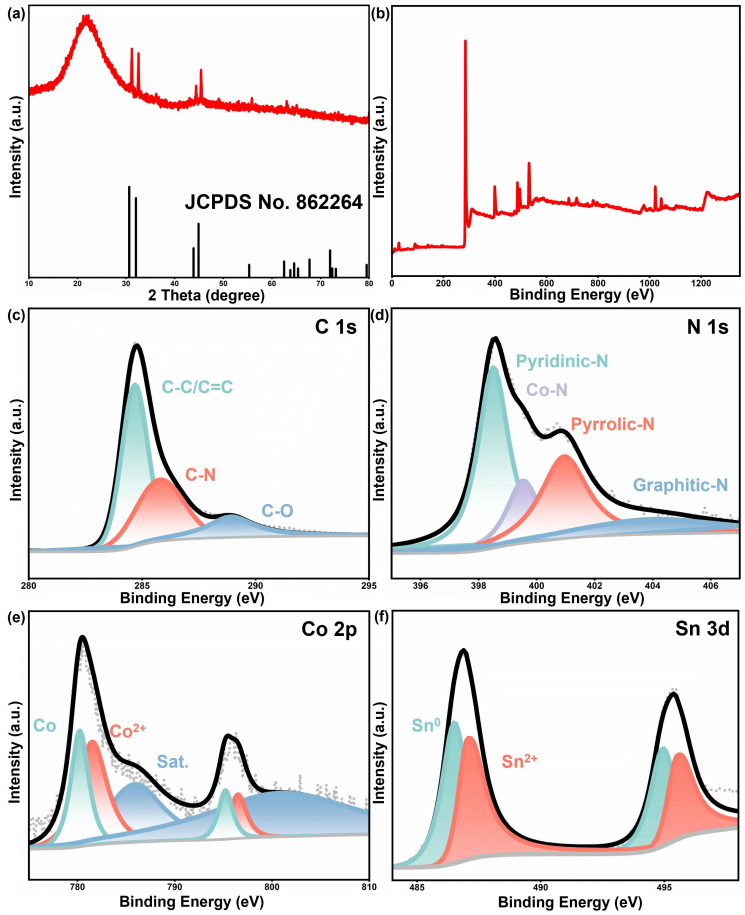

Fig. S13 XRD patterns (a) and XPS spectra (b-f) of CoSn@NC after 1000 CV cycles.

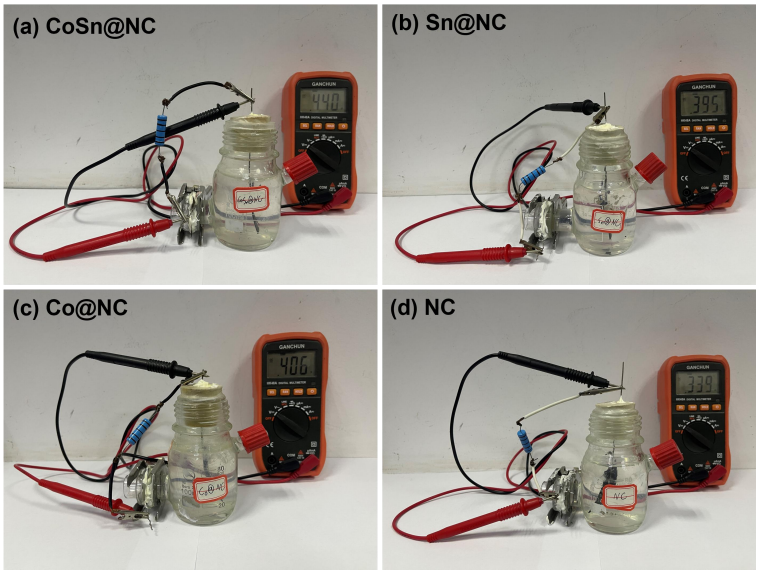

Fig. S14 The schematic diagrams of MFCs measurement.

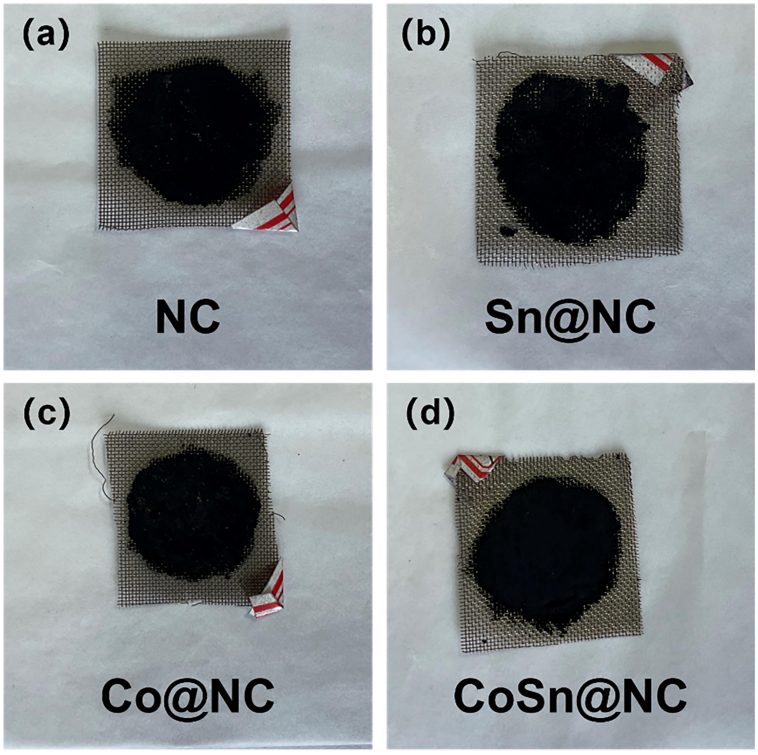

Fig. S15 Photographs of cathodes.

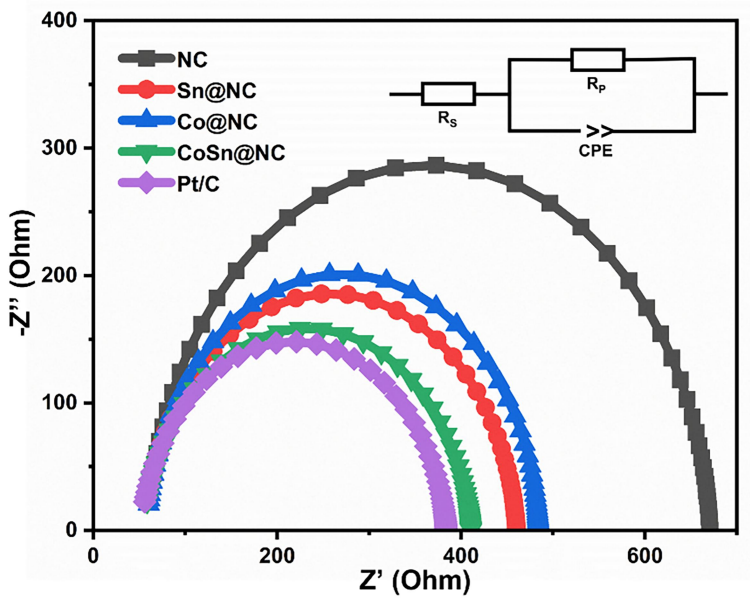

Fig. S16 Electrochemical impedance spectroscopic Nyquist plot for MFC devices with different catalysts.

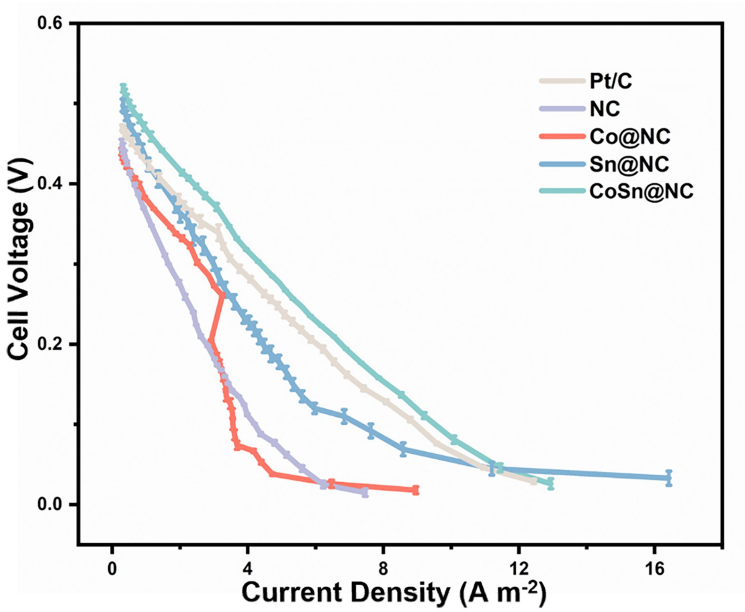

Fig. S17 Polarization curves of the MFCs.

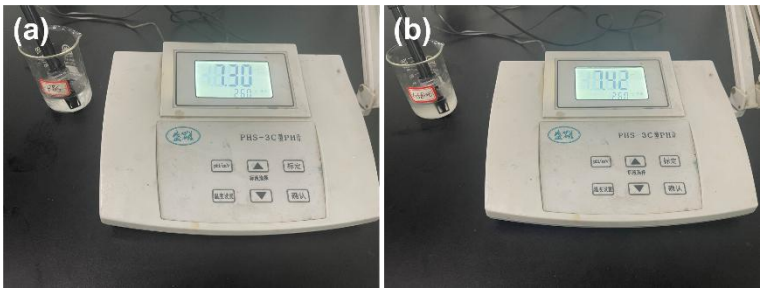

Fig. S18 pH of original PBS buffer (a) and CoSn@NC MFC (b).

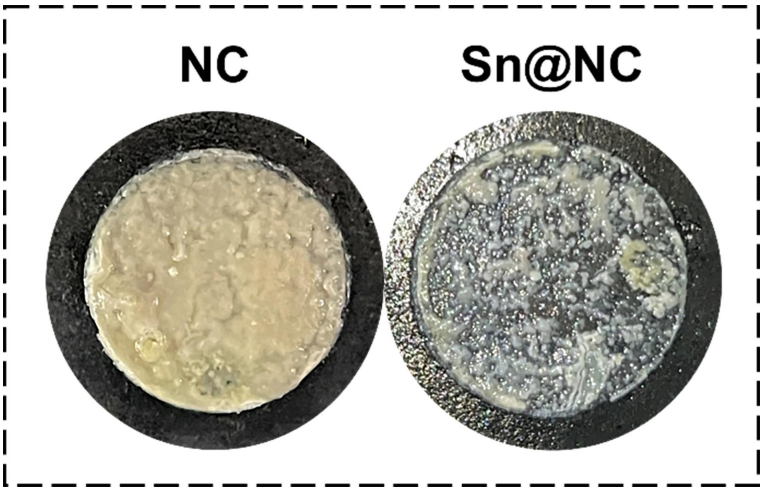

Fig. S19 Biofilm on the cathode surface of NC and Sn@NC after 500 h measurement.

Table S1. Relative amounts of pyridinic N, graphitic N, Pyrrolic N and Co-N.

Catalysts	Pyridinic N (%)	Graphitic N (%)	Pyrrolic N (%)	Co-N (%)
NC	53	23	25	/
Sn@NC	37	24	39	/
Co@NC	40	24	23	13
CoSn@NC	46	28	16	9

Table S2. The simulated data from EIS.

Catalysts	R_s (Ohm cm^{-2})	R_p (Ohm cm^{-2})	Z_w (Ohm cm^{-2})
NC	0.71	3.87	1.44
Sn@NC	0.70	3.60	1.34
Co@NC	0.63	2.90	1.12
CoSn@NC	0.56	2.66	0.57

Table S3. Summary of ORR activities of various catalysts in 0.1 M KOH.

Catalysts	Half-wave Potential (V)	Onset potential (V)	Limiting current density (mA cm^{-2})	Ref.
CoNi-SAs/NC	0.76	0.88	5	2
Ni_3C-GNRs	0.77	0.89	4.5	3
$MnCo_2O_4$/NCNTs	0.76	/	6.06	4
Fe_xCo_{9-x}-NHCS-V	0.80	/	/	5
ZIF-67@CoTMPP (800)	0.78	0.85	/	6
CoSn@NC	**0.84**	**0.90**	**7.13**	**this work**

Table S4. Summary of ORR efficiency of bimetallic catalysts.

Catalysts	Half-wave Potential (V)	Onset potential (V)	Limiting current density (mA cm^{-2})	Ref.
Cu_2O@Co/NC	0.80	0.89	3.80	7
Co_4/Fe_1@NC	0.83	0.98	/	8
Co-RuO_2/OCNT	0.82	/	/	9
CuCo@N/C	0.78	0.88	4.42	10
$MoFeC_x$-NC	0.82	0.95	/	11
CoSn@NC	**0.84**	**0.90**	**7.13**	**this work**

Table S5. Summary of antibacterial activities of various catalysts.

Antibacterial agent	**Microbial strain**	**Average inhibition diameter (mm)**	**Antimicrobial Substances**	**Ref.**
Zn-MOF	E. coli	8.6	ZnO nanoparticles	12
Ag−Fe−N/C	E. coli	3	Ag nanoparticles	13
(Fe/Co) Bi-MOFs	E. coli	12	(Fe/Co) Bi-MOFs nanoparticles	14
Cu-MOF	E. coli	11	Cu nanoparticles	15
Ac Zn-MOF	E. coli	14	released Zn^{2+}	16
CoSn@NC	**E. coli**	**12**	**released Sn^{2+} and generated ·OH**	**this work**

Table S6. Comparison of MFCs performance with different cathode catalysts.

Anode	Cathode	External resistance (Ω)	Output voltage (mV)	Power density (mW m^{-2})	Ref.
Carbon paper	Cu_2O@Co/NC	1000	430	1100	7
Carbon cloth	GO-Zn/Co (1:1)-800	1000	145	773	17
Carbon felt	MgO/GO	1000	354	755.63	18
Carbon paper	Ag/Co-N-C	/	502 ± 12	548 ± 12	19
Carbon felt	MPC-800	1000	470	240	20
Carbon cloth	**CoSn@NC**	**1000**	**460**	**1380**	**this work**

Reference

1. H. Xie, D. Jiang, H. Chen, X. Ma, X. Liu, Q. Qi and Y. Wang, Electron transfer and surface activity of NiCoP-wrapped MXene: cathodic catalysts for the oxygen reduction reaction, *Nanoscale*, 2023, **15**, 7430-7437.
2. X. Han, X. Ling, D. Yu, D. Xie, L. Li, S. Peng, C. Zhong, N. Zhao, Y. Deng and W. Hu, Atomically dispersed binary Co-Ni sites in nitrogen-doped hollow carbon nanocubes for reversible oxygen reduction and evolution, *Adv. Mater.*, 2019, **31**, 1905622.
3. X. Fan, Z. Peng, R. Ye, H. Zhou and X. Guo, M_3C (M: Fe, Co, Ni) nanocrystals encased in graphene nanoribbons: An active and stable bifunctional electrocatalyst for oxygen reduction and hydrogen evolution reactions, *Acs Nano*, 2015, **9**, 7407-7418.
4. Z. Wang, J. Huang, L. Wang, Y. Liu, W. Liu, S. Zhao and Z. Liu, Cation-tuning induced d-band center modulation on Co-based spinel oxide for oxygen reduction/evolution reaction, *Angew. Chem.-Int. Edit.*, 2022, **61**, e202114696.
5. S. Li, Y. Xie, B. Lai, Y. Liang, K. Xiao, T. Ouyang, N. Li and Z. Liu, Atomic modulation of Fe-Co pentlandite coupled with nitrogen-doped carbon sphere for boosting oxygen catalysis, *Chin. J. Catal.*, 2022, **43**, 1502-1510.
6. L. Wang, X. Jin, J. Fu, Q. Jiang, Y. Xie, J. Huang and L. Xu, Mesoporous non-noble metal electrocatalyst derived from ZIF-67 and cobalt porphyrin for the oxygen reduction in alkaline solution, *J. Electroanal. Chem.*, 2018, **825**, 65-72.
7. H. Chen, D. Jiang, H. Xie, Y. Liu, S. Li and Y. Wang, Cu_2O@Co/N-doped carbon as antibacterial catalysts for oxygen reduction in microbial fuel cells, *Environ. Sci.-Nano*, 2023, **10**, 158-165.
8. A. Han, W. Sun, X. Wan, D. Cai, X. Wang, F. Li, J. Shui and D. Wang, Construction of Co_4 atomic clusters to enable Fe-N_4 motifs with highly active and durable oxygen reduction performance, *Angew. Chem. -Int. Edit.*, 2023, e202303185.
9. Q. Lu, X. Zou, X. Wang, L. An, Z. Shao and Y. Bu, Simultaneous reactant accessibility and charge transfer engineering in Co-doped RuO_2-supported OCNT for robust rechargeable zinc-air batteries, *Appl. Catal. B-Environ.*, 2023, **325**, 122323.
10. X. Dong, J. Wang, X. Wang, J. Xu, J. Yang, W. Zeng, Y. Li, Y. Zhao, G. Huang, J. Wang and F. Pan, Bimetallic CuCo@nitrogen/carbon nanoparticles as a cathode catalyst for magnesium-air batteries, *ChemElectroChem*, 2022, **9**, e202200585.
11. X. Deng, S. Imhanria, Y. Sun, M. Zhang, Y. Cheng and W. Wang, Mo, Fe bimetallic carbide composite as high stability electrocatalyst for oxygen reduction reaction, *J. Environ. Chem. Eng.*, 2022, **10**, 108052.
12. F. Akbarzadeh, M. Motaghi, N. P. S. Chauhan and G. Sargazi, A novel synthesis of new antibacterial nanostructures based on Zn-MOF compound: design, characterization and a high performance application, *Heliyon*, 2020, **6**, e03231.
13. B. Lai, Z. Xiao, P. Jiang, Y. Xie, N. Li and Z. Liu, Two-dimensional Ag−Fe−N/C nanosheets as efficient cathode catalyst to improve power-generation performance

of microbial fuel cells, *ChemElectroChem*, 2022, **9**, e202101699.
14. F. T. Alshorifi, S. M. El Dafrawy and A. I. Ahmed, Fe/Co-MOF nanocatalysts: greener chemistry approach for the removal of toxic metals and catalytic applications, *ACS omega*, 2022, **7**, 23421-23444.
15. A. S. Abdelmoaty, A. A. El-Beih and A. A. Hanna, Synthesis, characterization and antimicrobial activity of copper-metal organic framework (Cu-MOF) and its modification by melamine, *J. Inorg. Organomet. Polym. Mater.*, 2022, **32**, 1778-1785.
16. M. Nakhaei, K. Akhbari, M. Kalati and A. Phuruangrat, Antibacterial activity of three zinc-terephthalate MOFs and its relation to their structural features, *Inorg. Chim. Acta*, 2021, **522**, 120353.
17. W. Yang, G. Chata, Y. Zhang, Y. Peng, J. Lu, N. Wang, R. Mercado, J. Li and S. Chen, Graphene oxide-supported zinc cobalt oxides as effective cathode catalysts for microbial fuel cell: High catalytic activity and inhibition of biofilm formation, *Nano Energy*, 2019, **57**, 811-819.
18. M. Li, S. Zhou and M. Xu, Graphene oxide-supported zinc cobalt oxides as effective cathode catalysts for microbial fuel cell: High catalytic activity and inhibition of biofilm formation, *Chem. Eng. J.*, 2017, **328**, 106-116.
19. P. Jiang, Z. Xiao, Y. Wang, N. Li and Z. Liu, Enhanced performance of microbial fuel cells using Ag nanoparticles modified Co, N co-doped carbon nanosheets as bifunctional cathode catalyst, *Bioelectrochemistry*, 2021, **138**, 107717.
20. Z. Zha, Z. Zhang, P. Xiang, H. Zhu, X. Shi and S. Chen, Porous graphitic carbon from mangosteen peel as efficient electrocatalyst in microbial fuel cells. *Sci. Total Environ.*, 2021, **764**, 142918.